A Two-Spot Sensor for Measurement of Dissipation by Means of Laser-Doppler Velocimetry*

JOHN TROWBRIDGE

Woods Hole Oceanographic Institution, Woods Hole, Massachusetts

YOGI AGRAWAL

Sequoia Scientific, Inc., Redmond, Washington

(Manuscript received 2 January 2003, in final form 10 November 2003)

ABSTRACT

An estimate of the dissipation rate for mechanical energy in a turbulent flow can be obtained by computing the variance of the temporal derivative of the fluid velocity measured at a single point. This technique is not suited to conventional laser-Doppler velocimetry because of inherent lower bounds on noise in the velocity measurements, which biases the dissipation estimates. A two-spot technique, described by George and Lumley, overcomes this difficulty. In this technique, laser-Doppler measurements of velocity are obtained at two points, which are separated in the spanwise direction by a distance larger than the size of the optical scatterers but smaller than the Kolmogorov scale. The covariance of the temporal derivative of the velocities measured at the two points provides an unbiased estimate of the dissipation, because the velocities at the two points are essentially identical, while the two noise records are uncorrelated. An oceangoing sensor based on this technique has been developed, and its success is demonstrated by experiments in the near-boundary region of a laboratory channel flow, where measurements of shear production provide a standard for evaluation of the dissipation estimates.

1. Introduction

An estimate of the dissipation rate for mechanical energy in a turbulent flow can be obtained from a point measurement of velocity by using

$$\epsilon = 15\nu\overline{\left(\frac{\partial u_1}{\partial x_1}\right)^2}, \tag{1}$$

provided that the dissipative motions are isotropic (Taylor 1935) and the frozen-turbulence hypothesis is valid (Taylor 1938; Lumley 1965), so that $\partial u_1/\partial x_1$ can be approximated by $-U_1^{-1}\partial u_1/\partial t$. Here, ϵ is the dissipation rate, ν is the kinematic viscosity, t is time, $\mathbf{x} = (x_1, x_2, x_3)$ is the position vector (with x_1 in the streamwise direction), $\mathbf{U} = (U_1, 0, 0)$ is the mean velocity, $\mathbf{u} = (u_1, u_2, u_3)$ is the fluctuating velocity, and an overbar denotes a mean value. Use of (1) to obtain estimates of dissipation from velocity measurements requires that the scale of the measurement volume be smaller than the Kolmogorov scale $\eta = (\nu^3/\epsilon)^{1/4}$, and that the sample rate be larger than approximately U_1/η (George and Lumley 1973).

In the ocean, (1) has been used to estimate dissipation from measurements of velocity obtained from heated films (e.g., Grant et al. 1962), which sense variations in the rate of heat transfer to determine velocity fluctuations, and from shear probes (e.g., Osborn 1974; Oakey 1982; Oakey and Elliot 1982), which sense flow-induced deflections of a small beam to determine velocity fluctuations. These techniques require calibrations of the relationship between the fluid velocity fluctuations and the quantity that is actually measured.

Oceanic estimates of dissipation based on (1) have also been obtained from acoustic travel time and acoustic Doppler measurements of fluid velocity (e.g., Shaw et al. 2001; Trowbridge and Elgar 2001) by means of inertial-range spectra; in addition, dissipation estimates have been obtained from range-gated pulse-to-pulse coherent Doppler sonar measurements (Veron and Melville 1999), which produce wavenumber spectra directly and do not require use of the frozen-turbulence hypothesis. These acoustic measurements often have sample volumes and sample rates insufficient to resolve the dissipative fluid motions, so that the resulting estimates of dissipation are indirect and dependent on a semiempirical model.

* Woods Hole Oceanographic Institution Contribution Number 10844.

Corresponding author address: Dr. John Trowbridge, Applied Ocean Physics and Engineering, Woods Hole Oceanographic Institution, 98 Water Street, MS 12, Woods Hole, MA 02543.
E-mail: jtrowbridge@whoi.edu

Oceanic measurements of dissipation have recently been obtained by means of particle-image velocimetry (PIV) (Doron et al. 2001), which requires no empirical calibration, resolves the dissipative scales under many conditions, and is capable of producing wavenumber spectra directly, without use of the frozen-turbulence hypothesis. However, PIV systems often require substantial hardware near the measurement region, which can produce flow disturbances in some applications.

Laser-Doppler velocimetry (LDV) appears to offer an attractive alternative to other methods of measuring dissipation in the ocean, because its small sample volume and rapid sample rate can, in principle, resolve the dissipative scales under many conditions, and because use of backscatter sensors and fiber-optic cables often permits minimization of flow disturbances. However, theoretical work and laboratory measurements (George and Lumley 1973) have shown that noise that is dependent on the positions and motions of the light-scattering particles produces unacceptably large biases in dissipation estimates produced by conventional laser-Doppler velocimetry. George and Lumley (1973) also described a solution to the noise problem: two laser-Doppler velocimeters, with sample volumes separated by a distance smaller than the Kolmogorov scale, measure essentially the same velocity but have uncorrelated noise. Thus, the covariance of the two records of $\partial u_1/\partial x_1$ produces an unbiased estimate of the dissipation. Clark (1970) reported an early laboratory implementation of this technique, and van Maanen et al. (1976) described a related technique in which two laser-Doppler measurements of velocity are obtained in the same sample volume.

Here we report a modern oceangoing version of a ''two spot'' laser dissipation sensor, based on the concept described by George and Lumley (1973). The sensor was tested in a laboratory channel, where estimates of shear production provide a standard for evaluation of the dissipation measurements. In addition, computations of a structure function $D_{11}(r_1)$, defined by

$$D_{11}(r_1) = \overline{[u_1(\mathbf{x} + \mathbf{e}_1 r_1) - u_1(\mathbf{x})]^2}, \qquad (2)$$

(e.g., Batchelor 1967) provide information about the ability of the sensor to resolve spatial scales. Here $\mathbf{r} = (r_1, r_2, r_3)$ is the separation, and $\mathbf{e}_1$, $\mathbf{e}_2$, and $\mathbf{e}_3$ are unit vectors in the x_1, x_2, and x_3 directions, respectively. In the following, the sensor, the laboratory measurements, and the analysis are described (section 2). Results are then presented and discussed (sections 3 and 4) and conclusions are summarized (section 5).

2. Methods

a. Laser dissipation sensor

The laser dissipation sensor (LDS) is a fiber-optic backscatter instrument that ''looks'' downward, in the x_3 direction, to provide independent measurements of the x_1 component of the velocity in two sample volumes, which are separated in the x_2 direction (Fig. 1). The system employs two separate diode lasers, both operating at 780 nm, each emitting approximately 150 mW of optical power. The beam from each laser is split and steered to form a parallel pair, so that the two lasers produce two parallel pairs of beams. One beam from each pair passes through a Bragg cell, which shifts its optical frequency by an amount equal to the Bragg cell drive frequency—a technique used to determine the direction of velocity. One Bragg cell operates at 38 MHz and the other operates at 43 MHz. The use of these two distinct frequency bands, each with a 1-MHz bandwidth, eliminates cross talk between the two velocity mea-

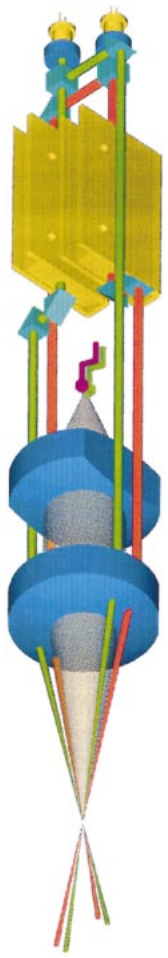

FIG. 1. Diagram of the two-spot laser dissipation sensor. As described in section 2a, the system employs two separate lasers, shown here in green and red. The beam from each laser is split and steered to form a parallel pair, so that the two lasers produce two parallel pairs of beams. One beam from each pair passes through a Bragg cell. The beam pairs pass through a focusing lens to form the two spots (intersection regions of each pair) where the two velocities are measured. The shaded cone displays the scattered light, which is received by the same lens. The two spots are imaged on to the tips of two multimode optical fibers, both placed at the back focal length of the receiving lens. The fibers carry the Doppler-shifted light signals to avalanche photodiode detectors and from there to two signal processors.

surements. The beam pairs pass through a focusing lens to form the two spots (intersection regions of each pair) where the velocity is measured. The scattered light is received through the same lens, and two spots are imaged onto the tips of two multimode optical fibers, both placed at the back focal length of the receiving lens. The fibers carry the Doppler-shifted light signals to avalanche photodiode detectors (APDs). The photocurrent from the two APDs is mixed between 38.256 and 43.256 MHz and then filtered through 1-MHz bandwidth filters, thus, placing a zero Doppler shift at a 256-kHz offset frequency. Each of these signals is then sent to a separate fast Fourier transform (FFT) signal processor. The photodiode detectors are sampled at twice the maximum frequency on the FFT. Each burst is 512 points long. A peak-detecting algorithm is used to determine the frequencies of the optical signals. The peak Fourier amplitude must satisfy two criteria—it must exceed a minimum threshold, and also it must be a minimum factor (25) times the mean spectral level. These two criteria ensure that noise is not identified as velocity. Each of the FFT processors provides an 8-bit measure of velocity. The centers of the two sample volumes are separated in the x_2 direction by 200 μm. The sample volumes are ellipsoids with nominal dimensions of 100 μm in the x_1–x_2 plane and 500 μm in the x_3 direction.

Tiny wedge prism pairs are used to form two spots at the required cross-stream spacing. A wedge prism deflects a beam by a small angle, equal to the incident angle times the excess refractive index of its material ($n - 1$). Two such prisms, placed together, can be used to add or subtract this deflection. Holding one prism fixed and rotating the other traces a circle. The diameter of the circle can be adjusted by rotating the first prism. In short, the wedge prism pair permits a change in direction of a laser beam by any angle between zero and twice the maximum deflection through one prism. In the optics employed for two spots, one pair of laser beams forms the first spot. Each beam of the second pair passes through the wedge prism pair. By adjusting the prism pair, each of the beams is deflected through a small angle [equal to (200 μm)/f, where f is the lens focal length] with respect to the original pair, so that the beams emerging after entering the focusing lens meet at 200 μm from the pair forming the first spot.

The imaging of the two spots on two optical fiber tips involves the use of a special fiber holder. This holder positions the tips precisely 200 μm apart. The receiving lens focal length equals that of the transmit lens so that the image of the two spots at the fiber tips has also a 200-μm separation. Alignment involves matching the fiber tip locations to the image locations of the two spots. Each of the receiving fiber is back lit (with a laser). After passing through the receive and transmit lenses, light emerging from the fiber tip (in the image plane) focuses at the desired measurement spot. Thus, the location of the measurement spots are defined by these back-lit fiber tips. Now, transmit optics are adjusted to force the beam-pair crossing at this location. The same procedure is repeated with the second fiber. It is imporant to note that the equal focal lengths of the two lenses ensures a one-to-one magnification of the object spots and image fiber tips. This design feature ensures that a given separation of the fiber tips results in an identical separation of the two spots. If a different magnification is employed, the corresponding change in spot separation can be achieved.

To reduce the path of the laser beams in turbid water, so that signal attenuation is minimized, and to reduce flow disturbance from the sensor housing, a tapered, water-filled ''snout'' is fixed to the instrument housing, and the optical beams pass through the snout before entering the water. The snout is a hollow frustum of a cone (a cone whose apex is sliced off parallel to its base), with a length of 0.100 m, a diameter of 0.075 m at its wide (upward) end, and a diameter of 0.006 m at its narrow (downward) end. After the large end is slipped on to the instrument housing (which has a flat glass pressure window), the snout is filled with clean water. A thin 6-mm-diameter paralleled glass window then closes the snout at the small end. The beams emerge from this snout without suffering misalignment because the small window itself has parallel surfaces. The sensing volume is 0.030 m below the narrow end of the snout.

b. Laboratory measurements

Tests of the LDS were conducted in the 17-m flume (Butman and Chapman 1989) in the Coastal Research Laboratory at the Woods Hole Oceanographic Institution. The 17-m flume is a recirculating system and has a straight test section with a smooth floor, glass walls, a length of 17 m, a breadth of 0.60 m, and a depth of 0.30 m. The flow is driven by a variable-speed pump. The velocity profile is homogenized at the upstream end of the test section by a baffle. An adjustable weir downstream of the test section constrains the relationship between water depth and discharge. Hydraulic jacks beneath the test section permit adjustment of the channel slope. Previous measurements (Trowbridge et al. 1989; Fries and Trowbridge 2003) have shown that the mean velocity and Reynolds stress in the 17-m flume at positions more than 10 m from the channel entrance and within 0.1 m of the channel centerline are consistent with established semiempirical results for steady uniform channel flow (Nezu and Rodi 1986), provided that the water depth is less than one-fourth of the channel breadth.

Measurements were obtained 12.8 m downstream of the entrance to the test section. The channel floor was horizontal. The depth-averaged along-channel velocity was nominally 0.2 m s^{-1}. The water depth at the measurement station was measured with a meter stick. The temperature and salinity of the water in the flume were measured with a platinum resistance thermometer and

a conductivity sensor, respectively. To provide optical scatterers, the flume was seeded with hollow glass spheres (manufactured by SonTek, Inc.) with a diameter and specific gravity of approximately 13.5 μm and 1.4, respectively. The particle concentration by volume was approximately 10^{-4}. The LDS was aligned with x_1, x_2, and x_3 in the along-channel, cross-channel, and vertical directions, respectively, so that the LDS sample volumes measured the along-channel velocity and were separated in the cross-channel direction. LDS measurements were obtained at $x_3 = 0.01$, 0.02, 0.03, 0.04, 0.06, and 0.08 m, where $x_3 = 0$ at the bottom. The sample rate was 500 Hz and the record lengths were 450 s, so that the number of samples at each height from each LDS spot was 225 000.

To test for flow disturbance by the LDS snout velocity measurements were obtained with a conventional LDV. The LDV is a fiber-optic backscatter system, manufactured by Dantec Measurement Technology, which is mounted outside the flume and focused through the flume's glass walls, so that it measures the along-channel velocity nonintrusively. The LDV sample volume is ellipsoidal with nominal dimensions of 4000 μm in the cross-channel direction and 200 μm in the along-channel and vertical directions. LDV measurements were obtained in the LDS measurement positions in two modes: one with the LDS absent (to determine the undisturbed flow) and one with LDS present but not operating (to determine the flow as influenced by the LDS). The measurements indicate that the mean along-channel velocity without and with the LDS in place differed by less than 3% (except at the lowest measurement position, where the difference was 6%), and that differences between disturbed and undisturbed inertial-range spectra were negligible.

c. Analysis

In preliminary analysis, velocities less than 0.08 m s^{-1} or greater than 0.30 m s^{-1} were identified and replaced by not-a-number (NaN), and velocities in each sample volume at each height which were more than 4 times the local standard deviation from the local mean were also identified and replaced by NaN. Only the valid measurements were used in the calculations of U_1, ϵ, and D_{11}.

Three estimates of dissipation based on (1) were obtained from the valid LDS measurements at each measurement height. The first estimate was obtained by computing 15ν times the variance of $\partial u_1/\partial x_1$ from record A, the second was obtained by computing 15ν times the variance of $\partial u_1/\partial x_1$ from record B, and the third was obtained by computing 15ν times the covariance of $\partial u_1/\partial x_1$ from records A and B. Here, $\partial/\partial x_1$ was estimated according to the frozen-turbulence approximation as $-(1/U_1)\partial/\partial t$, temporal derivatives were computed by differencing the velocity records, and A and B refer to the two sample volumes of the LDS.

Estimates of the shear production, defined by $-\overline{u_1u_3}\partial U_1/\partial x_3$, were used as a standard for evaluation of the dissipation estimates, because the shear production and dissipation are approximately equal in steady uniform channel flow if $x_3u_*/\nu > 30$ and $x_3/h < 0.4$ (Nezu and Nakagawa 1993), where u_* is the friction velocity and $x_3 = 0$ at the channel floor. In steady uniform channel flow for $x_3 > 30\nu/u_*$, the Reynolds stress $-\overline{u_1u_3}$ is given by

$$-\overline{u_1u_3} = u_*^2\left(1 - \frac{x_3}{h}\right), \tag{3}$$

where h is the water depth, and a semiempirical expression for the mean velocity is

$$U_1 = \frac{u_*}{\kappa}\ln(x_3) + \text{constant} + \frac{2\Pi}{\kappa}u_*\sin^2\left(\frac{\pi}{2}\frac{x_3}{h}\right), \tag{4}$$

(Nezu and Rodi 1986), where κ is the empirical von Kármán constant ($\kappa \simeq 0.40$) and Π is the empirical Coles parameter ($\Pi \simeq 0.2$ if $hu_*/\nu > 1000$). The corresponding expression for the shear production is

$$-\overline{u_1u_3}\frac{\partial U_1}{\partial x_3} = \frac{u_*^3}{\kappa x_3}\left(1 - \frac{x_3}{h}\right)\left[1 + \Pi\frac{\pi x_3}{h}\sin\left(\frac{\pi x_3}{h}\right)\right]. \tag{5}$$

An estimate of u_* was obtained by fitting measurements of U_1 to (4), and (5) was used to determine the shear production.

Estimates of $D_{11}(r_1)$ were computed for a range of r_1 at each measurement height. A structure function was used instead of the corresponding spectrum function because drop out complicated frequency-domain computations of spectra. The estimates of structure function were obtained by computing the covariance of $u_1(\mathbf{x} + \mathbf{e}_1r_1) - u_1(\mathbf{x})$ from records A and B. Here $u_1(\mathbf{x} + \mathbf{e}_1r_1)$ was calculated according to the frozen-turbulence approximation ($r_1 = -U_1\tau$, where τ is the temporal lag), and A and B refer to the two sample volumes of the LDS, as before. These two-spot estimates of $D_{11}(r_1)$ capitalize on the same noise cancellation concept as the two-spot estimates of dissipation. The presentation of $D_{11}(r_1)$ (section 3) is normalized according to Kolmogorov scaling, in which the statistical properties of the turbulence depend only on ϵ and ν (e.g., Tennekes and Lumley 1972). In this normalized presentation of D_{11}, ϵ is estimated from (5), based on the assumption that shear production equals dissipation.

The estimates of $D_{11}(r_1)$ are compared with three models. The first, a dissipation-range model valid for $r_1 \leq O(\eta)$, follows from (1) and (2) and is

$$D_{11}(r_1) = \frac{\epsilon r_1^2}{15\nu} + O(r_1^4). \tag{6}$$

The second and third models (see appendix A for details) are based on the semiempirical isotropic representations of turbulence spectra proposed by Pao (1965) and Nasmyth (see Oakey 1982). Both the Pao model

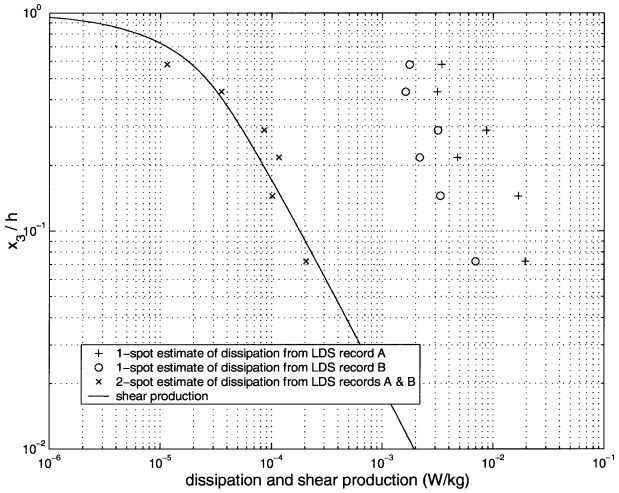

FIG. 2. Comparison of shear production with dissipation estimates obtained from the LDS. As explained in the text, records A and B are the two velocity records obtained from the individual LDS sample volumes. One-spot estimates of dissipation, obtained from (1) with a velocity record from a single sample volume, are between one and three orders of magnitude larger than the shear production, because of the large bias produced by noise. The two-spot estimates are consistent with the shear production, as expected, because of noise cancellation.

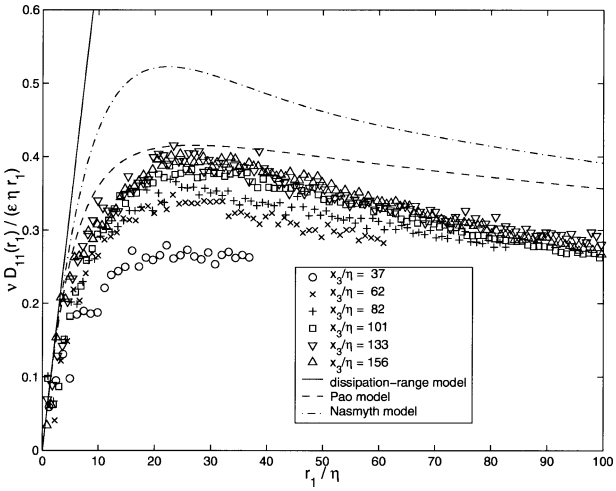

FIG. 3. Measured and modeled structure functions vs along-channel separation. All quantities are normalized by the Kolmogorov variables ϵ, ν, and $\eta = (\nu^3/\epsilon)^{1/4}$, where ϵ is estimated from (5) based on the assumption that shear production equals dissipation. The calculations are limited to $r_1 < x_3$. The Pao and Nasmyth models asymptote to the dissipation-range model (6) as $r_1/\eta \to 0$ and to the inertial-range model (7) as $r_1/\eta \to +\infty$. The measured structure functions are computed from the covariance of velocities measured by the two LDS sample volumes, in order to reduce the noise contribution. The measured structure functions are consistent with the dissipation-range model at small r_1/η and are approximately consistent with the Pao model at r_1/η on the order of 1 to a few 10s, provided that $r_1 \ll x_3$. The isotropic Pao model must fail at $r_1/x_3 = O(1)$, because proximity to the solid boundary introduces anisotropy at this scale.

and the Nasmyth model follow Kolmogorov scaling, and both models vary between the dissipation-range expression (6) at small r_1/η and the inertial-range expression

$$D_{11}(r_1) = \frac{54}{55}\cos\left(\frac{\pi}{3}\right)\Gamma\left(\frac{1}{3}\right)\alpha\epsilon^{2/3}r_1^{2/3}, \qquad (7)$$

at large r_1/η. Here Γ is the gamma function (e.g., Abramowitz and Stegun 1970). The isotropic Pao and Nasmyth models are expected to be valid only for $r_1 \ll x_3$.

3. Results

The water depth at the measurement position was 0.138 m. The kinematic viscosity, estimated as a function of the measured temperature and salinity from an empirical relationship (Siedler and Peters 1986), was 1.10×10^{-6} m^2 s^{-1}. The overall fractions of valid measurements (measurements identified as valid by the LDS internal processing and surviving the preliminary analysis procedure) were 0.52 and 0.35 for the two LDS sample volumes. The estimate of friction velocity obtained by fitting measurements of U_1 to (4) was 0.0103 $\pm$ 0.0008 m s^{-1} at 95% confidence.

Computations of shear production and dissipation (Fig. 2) indicate that conventional ''one spot'' estimates of ϵ, obtained from (1) with velocity records from each of the individual LDS sample volumes, are between one and three orders of magnitude larger than the shear production. In contrast, the two-spot estimates of dissipation, obtained from (1) with velocity records from both of the LDS sample volumes, agree well with the shear production. The one-spot estimates of dissipation, presumably dominated by noise, decrease slightly with increasing height above the bottom.

Plots of the structure function in the form $D_{11}(r_1)/r_1$ versus r_1 emphasize the contrast between the dissipation-range behavior (6), in which $D_{11}/r_1 \propto r_1$, and the inertial-range behavior (7), in which $D_{11}/r_1 \propto r_1^{-1/3}$. Plots of the structure functions at all measurement heights in this form (Fig. 3), normalized according to Kolmogorov scaling, indicate that the measured structure functions agree with (6) for small r_1/η, as expected from Fig. 2. At r_1/η on the order of 1 to a few 10s, the measured structure functions are approximately consistent with the Pao model, provided that $r_1/x_3 \ll 1$. The measured structure functions are less consistent with the Nasmyth model.

4. Discussion

The estimates of dissipation and shear production (Fig. 2) indicate success of the sensor based on the two-spot method for measuring dissipation by means of laser-Doppler velocimetry. The measured structure functions (Fig. 3) indicate consistency with the Pao model to the extent that can be expected, considering the limited separation between the Kolmogorov scale and the outer scale of the turbulence, which is proportional to

x_3. Any isotropic model of the structure function must fail at $r_1/x_3 = O(1)$.

The one-spot estimates of dissipation are roughly 3 times larger than estimates based on theoretical calculations of noise variance caused by finite transit time of particles through the sample volume and turbulent velocity gradients within the sample volume (George and Lumley 1973). The likely explanation is that noise in the LDS measurements is dominated not by the interactions between fluid velocities and optical scattering that were considered by George and Lumley (1973), but instead by electronic and optical noise. The one-spot estimates of dissipation are approximately consistent with a model in which the noise variance of the velocity measurements is constant, which produces a decay of dissipation estimates with increasing x_3 because of the inverse dependence on U_1 in the expression $\epsilon = (15\nu/U_1^2)\overline{(\partial u_1/\partial t)^2}$, which follows from (1) and the frozen-turbulence hypothesis.

A fundamental limitation on the measurement technique is imposed by the nonzero scale of the LDS sample volumes. George and Lumley (1973) considered the effect of the nonzero scale of a single sample volume. They used a Pao spectrum and considered an optical weighting function $w(\mathbf{x})$ defined by

$$w(\mathbf{x}) = \frac{1}{(2\pi)^{3/2}\sigma_1\sigma_2\sigma_3}\exp\left[-\left(\frac{x_1^2}{2\sigma_1^2} + \frac{x_2^2}{2\sigma_2^2} + \frac{x_3^2}{2\sigma_3^2}\right)\right], \tag{8}$$

finding (with some details depending on the precise geometry) that the largest of σ_1, σ_2, and σ_3 must be smaller than the Kolmogorov scale η in order to obtain 10% accuracy in dissipation estimates. The present sensor corresponds approximately to $\sigma_1 = \sigma_2 \simeq 25$ μm and $\sigma_3 \simeq 125$ μm, so that accurate measurements of dissipation are limited to $\eta > \sigma_3 = 125$ μm, or $\epsilon < 5.5 \times 10^{-3}$ W kg^{-1}, with $\nu = 1.1 \times 10^{-6}$ m^2 s^{-1}.

A second fundamental limitation on the two-spot measurement technique is imposed by the nonzero separation of the two sample volumes. To assess this effect, a model calculation was carried out (appendix B) in which the two sample volumes are points separated in the x_2 direction by a distance r_2 and the turbulence spectrum is represented by the Pao (1965) model. The calculations (Fig. 4) indicate that r_2 must be less than approximately 1.3η to produce a dissipation estimate within 10% of the true dissipation. The present sensor corresponds to $r_2 = 200$ μm, so that accurate measurements of dissipation are limited to $\eta > r_2/1.3 = 154$ μm, or $\epsilon < 2.4 \times 10^{-3}$ W kg^{-1}.

The present measurements indicate successful measurements of dissipation values as low as 10^{-5} W kg^{-1} (Fig. 2). A lower bound on the dissipation values that can be measured by the LDS cannot be determined from the present results.

The instantaneous quantity $(\partial u_1/\partial x_1)^2$, estimated by computing the product of the records of $\partial u_1/\partial x_1$ in the two sample volumes, is not lognormally distributed, as is usually expected in flows at high Reynolds numbers (e.g., Monin and Yaglom 1975). This result indicates that instantaneous estimates of $(\partial u_1/\partial x_1)^2$ have a relatively large noise component. The expected value of the noise is small, so that estimates of the mean dissipation are accurate, but the high noise level in individual estimates might preclude use of the LDS for examination of the intermittency of the dissipation, unless the measurements are suitably filtered (e.g., Yamazaki and Lueck 1990).

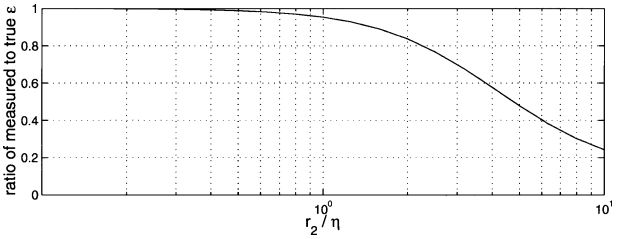

FIG. 4. Model calculation of the effect of the nonzero spanwise separation r_2 of the two LDS sample volumes. The calculation is based on a model in which each sample volume is a point and the turbulence spectrum is represented by the Pao model, as explained in appendix B.

Successful oceanic applications of the LDS require dissipation rates smaller than roughly 2×10^{-3} W kg^{-1} (as noted above) and light-scattering particles of sufficient size and concentration. Intuition suggests that particles smaller than the the wavelength of the optical interference pattern (approximately 10 μm in the present case) are required, but theory and measurements indicate that particles both smaller and larger than this limit produce modulations of the scattered light, and, therefore, meaningful Doppler measurements. In the case of the LDS, the particles should be smaller than the spot separation, so that the scattering processes in the two spots are statistically independent. Intuition suggests that successful direct measurements of dissipation require particle concentrations that are sufficient to ensure an interparticle spacing of roughly one Kolmogorov scale; in the laboratory tests reported here, the particle concentration was an order of magnitude larger than this value. Previous oceanic use of optical sensors (e.g., Agrawal et al. 1992; Trowbridge and Agrawal 1995; Doron et al. 2001) suggest that the most favorable application of the LDS will be in near-bottom or near-surface environments in the coastal ocean, where turbulence is energetic and suspended particles are abundant.

5. Conclusions

An oceangoing laser dissipation sensor based on the two-spot technique described by George and Lumley (1973) has been constructed. In this technique, two sample volumes separated in the spanwise direction measure

the along-stream component of the velocity, and the dissipation is computed from the covariance of the temporal derivatives of the two velocity records, which reduces the bias in the dissipation estimates that is introduced by the variability of the positions and velocities of the individual optical scatterers. The sensor has been tested in a laboratory channel, where estimates of shear production provide a standard for evaluation of the dissipation measurements. Measurements of dissipation and a structure function, which quantifies the spatial scales of the turbulence, are consistent with expectations, indicating that the sensor produces accurate estimates of the time-averaged dissipation. The sensor can produce accurate estimates of dissipation only when the Kolmogorov scale is larger than the scale of the individual sample volumes and larger than the distance by which the two sample volumes are separated, which limits applicability to dissipation rates less than approximately 2×10^{-3} W kg^{-1}. Noise levels in instantaneous estimates of the squared strain rate are high, which might limit use of the sensor in studies of the intermittency of the dissipation. Successful field application of this sensor will probably occur near the surface and bottom in the coastal ocean.

Acknowledgments. The National Science Foundation provided funding for this project. Chuck Pottsmith and Janet Fredericks conducted the laboratory experiment, and Janet Fredericks executed the preliminary data processing.

APPENDIX A

Models of the Structure Function

The structure function $D_{11}(r_1)$ can be represented by

$$D_{11}(r_1) = 2\int_{-\infty}^{+\infty} [1 - \cos(k_1 r_1)]F_{11}(k_1)\, dk_1, \quad \text{(A1)}$$

where $\mathbf{k} = (k_1, k_2, k_3)$ is the wavenumber vector and $F_{11}(k_1)$ is the longitudinal spectrum, related to the three-dimensional spectrum $E(k)$, where $k = |\mathbf{k}|$, by the isotropic expression

$$F_{11}(k_1) = \frac{1}{2}\int_{k_1}^{+\infty} \frac{k^2 - k_1^2}{k_1^3} E(k)\, dk \quad \text{(A2)}$$

(e.g., Batchelor 1967). The model proposed by Pao (1965) is

$$E(k) = \alpha\epsilon^{2/3}k^{-5/3} \exp\left[-\frac{3}{2}\alpha(k\eta)^{4/3}\right], \quad \text{(A3)}$$

where α is the empirical Kolmogorov constant. The model proposed by Nasmyth, given in tabular form by Oakey (1982), corresponds approximately to

$$F_{11}(k_1) = \begin{cases} (9/55)\alpha\epsilon^{2/3}k_1^{-5/3} & \text{for } k_1 \le k_0 \\ (9/55)\alpha\epsilon^{2/3}k_1^{-5/3} \exp\left\{\sum_{n=1}^{n=5} a_n[\log_{10}(k/k_0)]^n\right\} & \\ & \text{for } k_0 \le k_1, \end{cases} \quad \text{(A4)}$$

where $k_0\eta = 0.10$, $a_1 = -2.5708$, $a_2 = 3.1029$, $a_3 = -2.2918$, $a_4 = 0.7370$, and $a_5 = -0.0856$. The inertial-range expression (7) follows from substitution of (A4) into (A1) in the limit $k_1\eta \to 0$. The Pao model was calculated numerically from (A1), (A2), and (A3) and the Nasmyth model was calculated numerically from (A1) and (A4). The calculations are based on $\alpha = 1.53$.

APPENDIX B

Effect of Nonzero Separation of the Sample Volumes

Consider a model of the LDS in which point measurements of u_1 are separated by a distance r_2 in the x_2 direction. The statistics of the turbulent velocity fluctuations are assumed to be isotropic. The quantity determined by computing 15ν times the covariance of $\partial u_1/\partial x_1$ at the two measurement positions is not ϵ, as given by (1), but is instead a quantity ϵ_m, defined by

$$\epsilon_m = 15\nu\overline{\partial_{x_1}[u_1(\mathbf{x})]\partial_{x_1}[u_1(\mathbf{x} + r_2\mathbf{e}_2)]}. \quad \text{(B1)}$$

This quantity can be represented by

$$\epsilon_m = 15\nu\int_{-\infty}^{+\infty} dk_1 \int_{-\infty}^{+\infty} dk_2 \int_{-\infty}^{+\infty} dk_3\, k_1^2\phi_{11}(\mathbf{k})\cos(k_2 r_2), \quad \text{(B2)}$$

where $\phi_{11}(\mathbf{k})$ is a spectrum function (Batchelor 1967). The isotropic representation of $\phi_{11}(\mathbf{k})$ is

$$\phi_{11}(\mathbf{k}) = \frac{E(k)}{4\pi k^2}\left(1 - \frac{k_1^2}{k^2}\right) \quad \text{(B3)}$$

(Batchelor 1967). After substitution of (B3) into (B2) and introduction of polar coordinates [$k_2 = \sigma\cos(\theta)$ and $k_3 = \sigma\sin(\theta)$, where $0 \le \sigma < +\infty$ and $-\pi < \theta \le +\pi$], the k_2–k_3 integral can be evaluated, and the resulting expression can be written

$$\epsilon_m = \frac{15}{2}\nu\int_{-\infty}^{+\infty} k_1^2\, dk_1 \times \int_{k_1}^{+\infty} J_0(r_2\sqrt{k^2 - k_1^2})E(k)\frac{k^2 - k_1^2}{k^3}\, dk, \quad \text{(B4)}$$

where J_0 is a Bessel function (Abramowitz and Stegun 1970). This expression with $E(k)$ represented by the Pao model was evaluated numerically to produce Fig. 4. The ordinate in Fig. 4 is ϵ_m/ϵ.

REFERENCES

Abramowitz, M., and I. A. Stegun, 1970: *Handbook of Mathematical Functions.* National Bureau of Standards, U.S. Government Printing Office, 1046 pp.

Agrawal, Y. C., E. A. Terray, M. A. Donelan, P. A. Hwang, A. J. Williams, W. M. Drennan, K. K. Kahma, and S. A. Kitaigorodskii, 1992: Enhanced dissipation of kinetic energy beneath surface waves. *Nature,* **359,** 219–220.

Batchelor, G. K., 1967: *The Theory of Homogeneous Turbulence.* Cambridge University Press, 197 pp.

Butman, C. A., and R. J. Chapman, 1989: The 17-m flume at the Coastal Research Laboratory. Part 1: Description and user's manual. Woods Hole Oceanographic Institution Tech. Rep. 89-10, 31 pp.

Clark, W. H., 1970: Measurement of two-point velocity correlations in a pipe flow using laser velocimeters. Ph.D. thesis, University of Virginia, 151 pp.

Doron, P., L. Bertuccioli, J. Katz, and T. R. Osborn, 2001: Turbulence characteristics and dissipation estimates in the coastal ocean bottom boundary layer from PIV data. *J. Phys. Oceanogr.,* **31,** 2108–2134.

Fries, J. S., and J. H. Trowbridge, 2003: Flume observations of enhanced fine particle deposition to permeable sediment beds. *Limnol. Oceanogr.,* **48,** 802–812.

George, W. K., and J. L. Lumley, 1973: The laser-Doppler velocimeter and its application to the measurement of turbulence. *J. Fluid Mech.,* **60,** 321–362.

Grant, H. L., R. W. Stewart, and A. Moilliet, 1962: Turbulence spectra from a tidal channel. *J. Fluid Mech.,* **12,** 241–263.

Lumley, J. L., 1965: On the interpretation of time spectra measured in high intensity shear flows. *Phys. Fluids,* **8,** 1056–1062.

Monin, A. S., and A. M. Yaglom, 1975: *Statistical Fluid Mechanics: Mechanics of Turbulence.* Vol. 2. MIT Press, 874 pp.

Nezu, I., and W. Rodi, 1986: Open-channel flow measurements with a laser-Doppler anemometer. *J. Hydr. Eng.,* **112,** 335–355.

——, and H. Nakagawa, 1993: *Turbulence in Open-Channel Flows.* A. A. Balkema Publishers, 281 pp.

Oakey, N. S., 1982: Determination of the rate of dissipation of turbulent energy from simultaneous temperature and velocity shear microstructure measurements. *J. Phys. Oceanogr.,* **12,** 256–271.

——, and J. A. Elliott, 1982: Dissipation within the surface mixed layer. *J. Phys. Oceanogr.,* **12,** 171–185.

Osborn, T. R., 1974: Vertical profiling of velocity microstructure. *J. Phys. Oceanogr.,* **4,** 109–115.

Pao, Y. H., 1965: Structure of turbulent velocity and scalar fields at large wavenumber. *Phys. Fluids,* **8,** 1063–1075.

Shaw, W. J., J. H. Trowbridge, and A. J. Williams, 2001: Budgets for turbulent kinetic energy and scalar variance in the continental shelf bottom boundary layer. *J. Geophys. Res.,* **106,** 9551–9564.

Siedler, G., and H. Peters, 1986: Physical properties (general) of sea water. *Oceanography,* Vol. 3, *Geophysics and Space Research,* J. Sundermann, Ed., Numerical Data and Functional Relationships in Science and Technology Series, Group V, Springer-Verlag, 233–264.

Taylor, G. I., 1935: Statistical theory of turbulence. *Proc. Roy. Soc.,* **A151,** 421–444.

——, 1938: The spectrum of turbulence. *Proc. Roy. Soc.,* **A164,** 476–490.

Tennekes, H., and J. L. Lumley, 1972: *A First Course in Turbulence.* MIT Press, 300 pp.

Trowbridge, J. H., and Y. C. Agrawal, 1995: Glimpses of a wave boundary layer. *J. Geophys. Res.,* **100,** 20 729–20 743.

——, and S. Elgar, 2001: Turbulence measurements in the surf zone. *J. Phys. Oceanogr.,* **31,** 2403–2417.

——, W. R. Geyer, C. A. Butman, and R. J. Chapman, 1989: The 17-meter flume at the Coastal Research Laboratory. Part 2: Flow characteristics. Woods Hole Oceanographic Institution Tech. Rep. 89-11, 37 pp.

van Maanen, H. R. E., K. van der Molen, and J. Blom, 1976: Reduction of ambiguity noise in laser-Doppler velocimetry by a cross-correlation technique. *The Accuracy of Flow Measurements by Laser Doppler Methods, Proc. LDA-Symp. Copenhagen 1975,* P. Buchave et al., Eds., Copenhagen, Denmark, Technical University of Denmark, 81–88.

Veron, F., and W. K. Melville, 1999: Pulse-to-pulse coherent Doppler measurements of waves and turbulence. *J. Atmos. Oceanic Technol.,* **16,** 1580–1597.

Yamazaki, H., and R. Lueck, 1990: Why oceanic dissipation rates are not lognormal. *J. Phys. Oceanogr.,* **20,** 1907–1918.